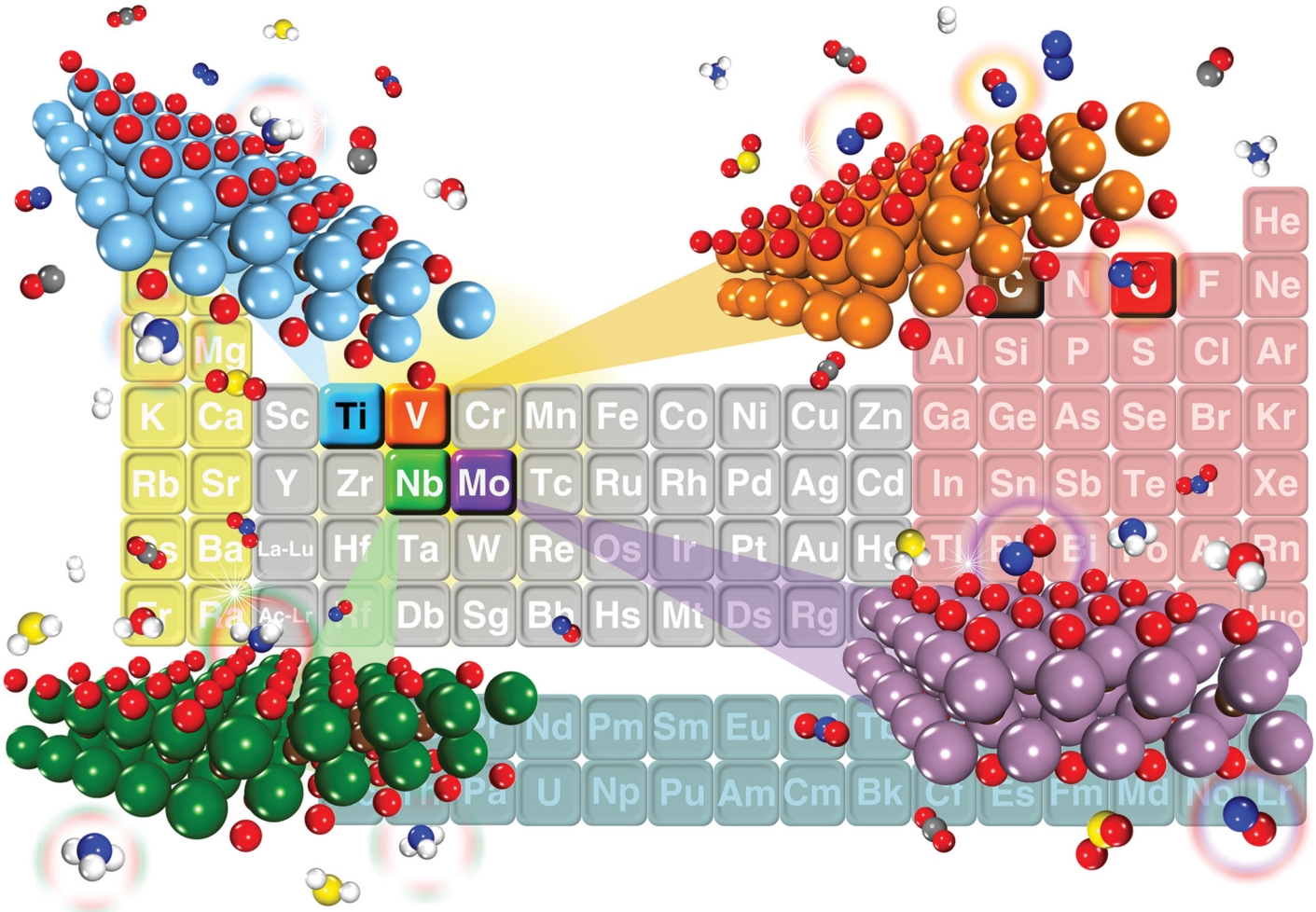

Showcasing research from Dr Anchalee Junkaew at the National Nanotechnology Center (NANOTEC), National Science and Technology Development Agency (NSTDA), Thailand

Enhancement of the selectivity of MXenes (M_2C, M = Ti, V, Nb, Mo) *via* oxygen-functionalization: promising materials for gas-sensing and -separation

This theoretical work reported that four MXenes (*i.e.* M_2C (M =Ti, V, Nb, Mo)) are very reactive and are attractive for catalytic applications. The O-functionalized MXenes are less reactive but more selective to particular gas species than the pristine MXenes. Our findings proposed the feasibility of using these O-MXenes in gas-separation, -capture, -sensing and catalytic applications.

As featured in:

See A. Junkaew and R. Arróyave, *Phys. Chem. Chem. Phys.*, 2018, **20**, 6073.

ROYAL SOCIETY OF CHEMISTRY

rsc.li/pccp

Registered charity number: 207890

PCCP

PAPER

View Article Online
View Journal | View Issue

Cite this: *Phys. Chem. Chem. Phys.*, 2018, **20**, 6073

Enhancement of the selectivity of MXenes (M_2C, M = Ti, V, Nb, Mo) *via* oxygen-functionalization: promising materials for gas-sensing and -separation†

A. Junkaew *[a] and R. Arróyave[b]

Received 25th December 2017,
Accepted 1st February 2018

DOI: 10.1039/c7cp08622a

rsc.li/pccp

Two-dimensional graphene-like materials, namely MXenes, have been proposed as potential materials for various applications. In this work, the reactivity and selectivity of four MXenes (*i.e.* M_2C (M = Ti, V, Nb, Mo)) and their oxygen-functionalized forms (*i.e.* O-MXenes or M_2CO_2) toward gas molecules were investigated by using the plane wave-based Density Functional Theory (DFT) calculations. Small gas molecules, which are commonly found in flue gas streams, are considered herein. Our results demonstrated that MXenes are very reactive. Chemisorption is a predominant process for gas adsorption on MXenes. Simultaneously dissociative adsorption can be observed in most cases. The high reactivity of their non-functionalized surface is attractive for catalytic applications. In contrast, their reactivity is reduced, but the selectivity is improved upon oxygen functionalization. Mo_2CO_2 and V_2CO_2 present good selectivity toward NO molecules, while Nb_2CO_2 and Ti_2CO_2 show good selectivity toward NH_3. The electronic charge properties explain the nature of the substrates and also interactions between them and the adsorbed gases. Our results indicated that O-MXenes are potential materials for gas-separation/capture, -storage, -sensing, *etc.* Furthermore, their structural stability and SO_2-tolerant nature are attractive properties for using them in a wide range of applications. Our finding provides good information to narrow down the choices of materials to be tested in future experimental work.

1. Introduction

Enhancement of the selectivity, performance, stability and durability of adsorptive and catalytic materials under proper working conditions is still challenging for many energy and environmental technologies such as SO_x/NO_x removal from flue gas streams, hydrogen storage, gas purification, gas sensors, CO_2 capture, N_2 fixation, *etc.*[1–5] Besides conventional metal- and metal-oxide based materials, numerous two-dimensional (2D) materials other than graphene such as silicon carbide (SiC), hexagonal boron nitride (h-BN), transition-metal dichalcogenides (TMDs *i.e.* MoS_2 and WS_2), transition metal carbides (TMCs), silicene, stanene, germanene, *etc.* have been extensively explored and utilized in those applications.[6–9]

Currently, graphene-like materials, so-called MXenes, have gained a lot of attention as they have been proposed as promising materials for many applications.[10–16] These materials are layers of transition metal-carbides and -carbonitrides. Nowadays, a chemical etching procedure[17] has become a widely used technique for fabricating MXene sheets ($M_{n+1}X_n$ (n = 1, 2, 3)) from parent MAX phases ($M_{n+1}AX_n$), where 'M' is a transition d-metal, 'A' is a p-element and 'X' is C and/or N. Since a hydrofluoric acid (HF) solution is used in the chemical etching process, the O, F and OH functional groups are generally found on the surfaces of exfoliated MXenes.[11,17] Terminated MXenes are denoted by $M_{n+1}X_nT_x$, where T is a terminating group. Those functional groups can be eliminated by heat treatment.[18,19] Now, many MXenes such as Ti_2C, Ti_3C_2, V_2C, Nb_2C, Nb_4C_3, $(Nb_{0.8}Zr_{0.2})_4C_3$, $(Nb_{0.8}Ti_{0.2})_4C_3$, $(V_{0.5},Cr_{0.5})_3C_2$, Ta_4C_3, $(V_{0.5},Cr_{0.5})_3C_2$, $(Ti_{0.5},Nb_{0.5})_2C$, Ti_3CN, Mo_2C, Zr_3C_2 and Ti_4N_3 and their functionalized forms have been successfully synthesized in laboratory.[17,20–25] It is likely that new MXenes will be fabricated in the future due to a variety of choices of constitute elements of parent MAX phases. In addition, the ceramic nature of MXenes allows them to be chemically and mechanically stable.[10]

From literature studies, changing the constituents does not only play a key role in affecting MXenes' properties, but altering the functional groups also plays an important role in their electronic, optical, thermal, electrochemical, catalytic,

[a] *National Nanotechnology Center (NANOTEC), National Science and Technology Development Agency (NSTDA), Pathum Thani 12120, Thailand. E-mail: anchalee@nanotec.or.th*

[b] *Department of Materials Science and Engineering, Texas A&M University, College Station, TX 77843-3003, USA*

† Electronic supplementary information (ESI) available. See DOI: 10.1039/c7cp08622a

mechanical properties, *etc.* While pristine MXenes present the metallic nature, their electronic properties are tunable as some of them exhibit metallic or semiconducting characteristics upon functionalization.[10] In the Ti_2C, Hf_2C and Zr_2C cases, O-functional groups result in the semiconducting nature, while –F and –OH groups still retain their metallic nature as observed in their non-functionalized phases.[26] Those aforementioned aspects open more opportunities to tailor these materials to a wide variety of applications.

According to prior work, terminated MXenes exhibit good selectivity toward specific gases or compounds. Some of them have been proposed as candidates for sensor applications. For example, Ti_2CO_2 and Zr_2CO_2 revealed good selectivity toward NH_3.[27,28] Oxygen-terminated Sc_2C was proposed for SO_2 sensing.[29] Recently, terminated Ti-based MXene nanosheets ($Ti_3C_2T_x$) integrating with flexible polyimide films have been proposed as a p-type sensing material for the detection of ethanol, methanol, acetone, and ammonia gas at room temperature by Lee *et al.*[30] They found that a fabricated sensor showed good response towards NH_3 due to the large adsorption energy between NH_3 and $Ti_3C_2T_x$. As demonstrated in those studies, these emerging materials become potential candidates in sensing applications due to their particular electronic properties, hydrophilic surface, biocompatibility and stability.[31] Terminated MXenes have also been investigated as adsorptive materials for pollutant or hazardous abatement. V_2CT_x was used for capturing uranium[32] and uranyl species,[33] which are nuclear wastes. The experimental work reported that $Ti_3C_2T_x$ nanosheets are good sorbents for Cu ions in aqueous solutions.[34] Owing to their outstanding characteristics, terminated MXenes reveal great performance in various applications such as electrodes for Li- or Na-ion batteries,[13,35–37] thermoelectric[15] and photocatalytic water splitting,[14] catalytic CO_2 reduction,[16] solid lubricants,[38] pollutant abatement,[32,33] *etc.*

The adsorption capability is one of the key factors that reveals the selectivity of an individual compound over other species on an adsorbent. This property is also one of the descriptors to determine the activity of a catalyst.[39] So far, the adsorption property calculated by theoretical methods has been used as a tool for screening and discovering new adsorbents and new catalysts. To date, a full understanding of various MXenes and their functionalized forms is still limited. Therefore, a deeper understanding and further investigations are needed in order to bring these materials closer to applications. In this work, we aim to study the gas adsorption ability of different gas species on MXenes and O-MXenes by using a periodic Density Functional Theory (DFT) method. Ti_2C, V_2C, Nb_2C and Mo_2C and their O-functionalized forms were investigated in this work. Ten gas molecules such as H_2, H_2O, CO, CO_2, N_2, NO, NO_2, NH_3, H_2S and SO_2 are chosen as adsorbates herein. O_2 is also considered in bare MXene cases. Structural and electronic charge analyses were performed for understanding the nature of these materials and the interactions between them and the adsorbates. Our results are beneficial for guiding the feasibility of using these materials in gas-storage, -separation/purification, -sensors, catalysis or other applications.

2. Computational methods

Adsorption of the ten molecules on MXenes and O-MXenes was examined by using periodic DFT calculations implemented in the Vienna *ab initio* Simulation Package (VASP) code.[40,41] The Perdew–Burke–Ernzerhof (PBE)[42] with a projector-augmented wave (PAW)[43] method was used in this work. For the dispersion contribution, Grimme's DFT-D3[44] was applied. The PBE with D3 correction has been applied in many MXenes and other studies.[45–48] It provided the best agreement with highly accurate Coupled Cluster Singles Doubles with perturbative Triples (CCSD(T)) calculations for the physisorption of H_2 on the metal oxide models.[48] An energy cutoff of 520 eV and an energy convergence of 1×10^{-6} eV were used for optimization criteria. Gaussian smearing with $\sigma = 0.1$ was applied. Monkhorst–Pack scheme for *k*-point grids of $5 \times 5 \times 1$ and $15 \times 15 \times 1$ were used for optimization and density of state calculations. A (3×3) slab is separated from its replicas by 15 Å of vacuum. A three dimensional structure of the MXene slab is presented in Fig. 1. The electronic charge properties such as density of states (DOS), electron localization function (ELF),[49] charge difference and Bader charge[50,51] were analyzed.

The adsorption energy (E_{ad}) can be obtained from the following equation:

$$E_{ad} = E^{complex}_{adsorbate-substrate} - E^{isolated}_{substrate} - E^{isolated}_{adsorbate}$$

where $E^{complex}_{adsorbate-substrate}$ is the total energy of the adsorbate–substrate complex. $E^{isolated}_{substrate}$ and $E^{isolated}_{adsorbate}$ are the total energies of a bare substrate and an isolated adsorbate, respectively.

3. Results and discussion

3.1 MXenes and O-functionalized MXenes

First, four MXenes and their O-functionalized structures were optimized for using as the substrates in the adsorption calculations. Top and side views of MXene are illustrated in Fig. 1. According to prior work, the functional groups prefer hollow sites than atop metal sites.[26] Thus, two possible adsorption sites for O atoms, which are an fcc site or a hollow metal site (hollow-M site, H^M) and a hcp site or a hollow carbon site (hollow-C site, H^C), are considered in this work (see Fig. 1). In each O-MXene, the binding energy (E_b) per oxygen atom was calculated to compare the stability of oxygen termination at the H^M and H^C sites. On the other hand, decreasing of E_b indicates a stronger binding strength between the O atoms and MXenes surfaces. E_b can be calculated from $E_b = (E_{O\text{-}MXene} - E_{MXene} - nE_O)/n$. $E_{O\text{-}MXene}$, E_{MXene}, and

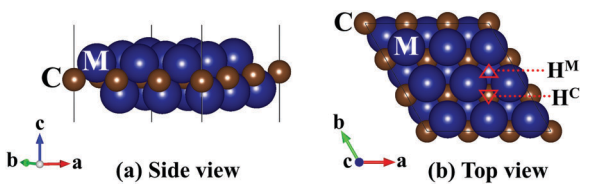

Fig. 1 (a) Side view and (b) top view of M_2C. Blue and brown balls represent metal (M) and carbon (C) atoms, respectively.

Table 1 Atomic distances (r) in Å of MXene and O-MXene supercells, where M, C and O denote metal, carbon and oxygen atoms, respectively. The two adsorption sites are the hollow-M (H^M) and hollow-C (H^C) sites. The E_b values of O-MXenes calculated using the PBE method are given in eV per O atom

M_2C	$r_{(M-C)}$ (Å)	M_2CO_2	Site	E_b (eV/O)	$r_{(M-C)}$ (Å)	$r_{(M-O)}$ (Å)
Ti_2C	2.10 2.1[52]	Ti_2CO_2	H^M	−8.40	2.19 2.19[45] 2.19[53]	1.97 1.98[45] 1.98[53]
			H^C	−8.21	2.25	1.97
V_2C	2.00	V_2CO_2	H^M	−7.45	2.06 2.05[45]	1.96 1.96[45]
			H^C	−7.14	2.05	1.98
Nb_2C	2.17 2.198[54]	Nb_2CO_2	H^M	−7.83	2.22 2.21[45]	2.12 2.13[45]
			H^C	−7.57	2.22	2.13
Mo_2C	2.08 2.15[55]	Mo_2CO_2	H^M	−7.03	2.0–2.5	1.9–2.3
			H^C	−7.42	2.16 2.16[45]	2.06 2.06[45]

E_O are the total energies of O-MXene, pristine MXene and the oxygen atom, respectively. n is the total number of oxygen atoms on the O-MXene's surface.

The atomic distances of optimized MXene and optimized O-MXenes are given in Table 1. The bond lengths of metal–carbon and metal–oxygen are denoted by $r_{(M-C)}$ and $r_{(M-O)}$, respectively. In all cases, the preference adsorption site is the H^M site except for the Mo_2CO_2 system. The preference termination sites of Ti_2CO_2, V_2CO_2 and Nb_2CO_2 agree with ref. 26 and 45. The preference site of oxygen termination on Mo_2C is the same as reported in the literature.[45,56] The $r_{(M-C)}$ and $r_{(M-O)}$ values in Ti_2CO_2 compare well with the values calculated using PBE[53] and PBE-D3[45] methods. According to the results from the HSE hybrid functional, 2.17 Å of $r_{(M-C)}$ and 1.96 Å of $r_{(M-O)}$ were reported in the same ref. 53. Since the O termination at the H^M site on Mo_2C leads to a distorted structure after optimization, the bond distances of Mo–C and Mo–O are varied in the range of 2.0–2.5 Å and 1.9–2.3 Å, respectively. The O atom at the H^M site is less stable than at another site. The order of E_b is Ti_2CO_2 (−8.40 eV/O) < Nb_2CO_2 (−7.83 eV/O) < V_2CO_2 (−7.45 eV/O) < Mo_2CO_2 (−7.42 eV/O). The stable forms of four O-MXenes were used as the substrates for the gas adsorption calculations.

In addition, the ELF properties of four MXenes were elucidated and the results are illustrated in Fig. 2. ELF can be used to distinguish the types of chemical bonding in solids.[57–59] The ELF value of 0.5, which is represented by the yellow region in Fig. 2, identifies the homogenous electron gas-like behavior in that region.[49,60] In Fig. 2a–c, the regions, which have an ELF value of 0.5, exist at the hollow metal sites on Ti_2C, Nb_2C and V_2C. In contrast, the yellow regions can be observed around the C sites in the case of Mo_2C, which results in different preference sites for oxygen adsorption. Interestingly, the preference site corresponds to the ELF properties of pristine MXenes. The results clarify that the free electron regions tend to be the preferred trapping site for oxygen atoms.

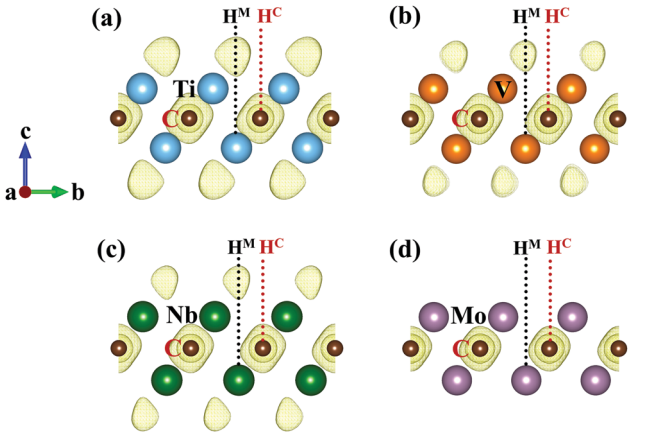

Fig. 2 ELF isosurface represented by the yellow regions of pristine MXenes (a) Ti_2C, (b) V_2C, (c) Nb_2C and (d) Mo_2C. Isovalue is 0.5.

3.2 Gas adsorption on MXenes

Gas adsorption on bare MXenes calculated using the PAWPBE method is discussed in this part. As a result, the lowest E_{ad} values of the eleven molecules adsorbed on the four bare MXene surfaces are compared in Fig. 3. The dissociative adsorption indicates the adsorption process that a gas molecule is simultaneously dissociated on a substrate upon adsorption. On the other hand, the molecular adsorption indicates the process where an adsorbate retains its molecular form when it is adsorbed on a surface. The dissociative adsorption and the molecular

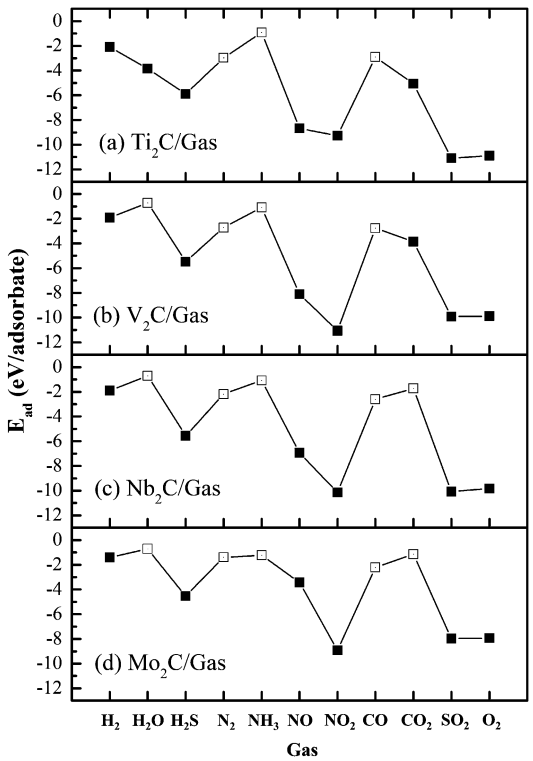

Fig. 3 Comparison of the E_{ad} values of gas adsorption on (a) Ti_2C, (b) V_2C, (c) Nb_2C and (d) Mo_2C calculated by PBE. Filled and open squares denote the dissociative- and molecular-adsorption, respectively.

adsorption are represented by filled and open squares. The calculated E_{ad} values are given in Table S1 in the ESI.† The selected configurations of gas-adsorbed MXenes and the calculated bond distances are given in Fig. S1–S4 in the ESI.†

As a result, most gas species are dissociated when they are adsorbed on MXene surfaces. As illustrated in Fig. S1–S4 in the ESI,† the dissociated H atoms move to one H^M site and the nearest H^C site when it is attached *via* a side-on adsorption mode (*i.e.* parallel) around the hollow sites in all MXenes. It is worth mentioning that H_2 is not attached with the hollow sites by an end-on binding configuration. H_2 is molecularly adsorbed as a side-on binding mode on the atop metal site which is physisorption. The E_{ad} values of H_2 molecules on the top metal sites of Ti_2C, V_2C, Nb_2C and Mo_2C are −0.34 eV, −0.67 eV, −0.51 eV and −0.78 eV, respectively. The H–H bond lengths are in the range of 0.85–0.89 Å, which are longer than the 0.75 Å of an isolated H_2 molecule. According to the H–H bond lengths, this activated H–H bond on a metal site is called the Kubas mode of adsorption.[61,62] The dissociative and molecular adsorption configurations of H_2 on Ti_2C and V_2C in this work agree well with the observations of Hu *et al.*[63] According to the work of Hu *et al.*, the average E_{ad} values of H_2 on the atop Ti and V sites of pre-adsorbed H atoms on the Ti_2C (3 × 3) and V_2C (3 × 3) surfaces are −0.27 eV and −0.24 eV, respectively.[63] As shown in Fig. S1–S4 in the ESI,† H_2S, NO, NO_2, SO_2 and O_2 are dissociated when they adsorb in parallel on MXenes. In Ti_2C, SO_2 presents the strongest interaction with an E_{ad} of −11.09 eV. In V_2C, Nb_2C and Mo_2C, the lowest E_{ad} value can be observed for NO_2 adsorption compared to other gas species. The dissociated atoms move to the nearby hollow sites as shown in Fig. S1–S4 in the ESI.† The simultaneous dissociation of O_2 indicates that MXenes are oxidized easily when O_2 exists. This agrees well with the barrier-less O_2 dissociation on Ti_2C observed in other previously published studies.[64,65] Fredrickson *et al.* reported that bare Ti_2C and bare Mo_2C are not stable unless applying a potential.[65]

There are N_2, $NH_3$and CO molecules which are still in the molecular forms in all MXenes. For NH_3, it prefers the top site of the metal with E_{ad} in the range of −1.23 eV to −0.91 eV. The adsorption strength is in the following order NH_3/Mo_2C > NH_3/V_2C ≈ NH_3/Nb_2C > NH_3/Ti_2C. The calculated E_{ad} values of NH_3/V_2C (−1.08 eV) and NH_3/Nb_2C (−1.07 eV) reveal similar ranges to the calculated Gibbs free binding energies (ΔG_b) of NH_3/V_3C_2 (−0.92 eV) and NH_3/Nb_3C_2 (−1.16 eV), at 298.15 K.[47] As presented in Fig. S1–S4 in the ESI,† the bonds of adsorbed-N_2 and -CO are activated and are lengthened from 1.11 Å to 1.14 Å of their gas phases, respectively. In the N_2/Ti_2C system, the activation of the N–N bond and the calculated E_{ad} of −2.97 eV are similar with the N_2 adsorption behavior on Ti_3C_2, which exhibits −2.57 eV of ΔG_b at 298.15 K.[47] For the H_2O adsorption, the dissociated adsorption can be observed in Ti_2C only. One H and –OH are separated to different H^M sites with an E_{ad} of −3.84 eV as illustrated in Fig. S1c in the ESI.† At the same time, the H_2O adsorption in the rest of the MXenes prefers molecular adsorption on the top metal site with E_{ad} ∼ −0.7 eV. In contrast, H_2O is molecularly adsorbed on Ti_3C_2 with ΔG_b of −1.35 eV at 298.15 K.[47] Similar to our V_2C case, H_2O is adsorbed molecularly on V_3C_2 with ΔG_b of −0.96 eV.[47] For the CO_2 adsorption, the CO_2 molecules are broken into O and CO on the Ti_2C and V_2C surfaces as presented in Fig. S1n and m (ESI†), respectively. In Nb_2C and Mo_2C, the C atom of the CO_2 molecule is located at the H^M site. The O–C–O angles of CO_2 are distorted from 180° to 130.8° and 132.8° on Nb_2C and Mo_2C, respectively.

In summary, these dissociative aspects result in a high adsorption strength or low E_{ad} value. They also signify the high reactivity but low selectivity of the bare MXene surfaces. On the other hand, the high reactivity is an advantage for using them as catalysts. For example, their metallic nature and their favorable CO_2 adsorption would be useful for catalytic CO_2 reduction as observed in Cr_3C_2 and Mo_3C_2 for the conversion of CO_2 into CH_4.[66] Azofra *et al.*[47] reported that the activation of a N–N bond promotes the catalytic conversion of N_2 into NH_3 under mild conditions. From their investigation, V_3C_2 and Nb_3C_2 revealed good catalytic properties for an electrocatalytic reduction of N_2 into NH_3. N_2 chemisorption is more preferable than H_2O and CO_2 adsorption resulting in the good selectivity of V_3C_2 towards N_2 conversion.[47] Therefore, our gas adsorption on bare MXenes suggest that these MXenes might be candidates to be tested for N_2 fixation into NH_3, the catalytic CO_2 reduction to fuels, *etc.*

3.3 Gas adsorption on O-functionalized MXenes

In this section, gas adsorption on four O-functionalized MXenes is discussed. The calculated E_{ad} values of ten gases over four O-MXenes are plotted and compared as depicted in Fig. 4. From the E_{ad} values calculated using the PBE method, most molecules are weakly adsorbed on O-MXenes. Herein, the van der Waals correction implemented in the DFT-D3 method were applied to include the non-bonded interactions. The results from PBE and PBE-D3 are plotted and compared in Fig. 4a and b, respectively. The calculated E_{ad} values are summarized in Table S1 in the ESI.† The most stable configurations of gas-adsorbed surfaces, and the bond distances are given in Fig. S5–S8 in the ESI.†

Fig. 4a compares the calculated E_{ad} values of the ten gas molecules on Ti_2CO_2. The most stable configuration of each gas on Ti_2CO_2 and its E_{ad} are displayed in Fig. S5 (ESI†). As a result, the tendency of gas adsorption strength from high to low is NH_3/Ti_2CO_2 (E_{ad} = −0.37 eV) > SO_2/Ti_2CO_2 (E_{ad} = −0.26 eV) ≈ NO/Ti_2CO_2 (E_{ad} = −0.25 eV) ≈ H_2S/Ti_2CO_2 (E_{ad} = −0.24 eV) > H_2O/Ti_2CO_2 (E_{ad} = −0.21 eV) ≈ CO_2/Ti_2CO_2 (E_{ad} = −0.20 eV) > NO_2/Ti_2CO_2 (E_{ad} = −0.17 eV) > N_2/Ti_2CO_2 (E_{ad} = −0.13 eV) ≈ CO/Ti_2CO_2 (E_{ad} = −0.13 eV) > H_2/Ti_2CO_2 (E_{ad} = −0.07 eV). From a prior work, the E_{ad} values of NH_3/Ti_2CO_2, CO_2/Ti_2CO_2, NO_2/Ti_2CO_2, N_2/Ti_2CO_2 and H_2/Ti_2CO_2 are −0.37 eV, −0.14 eV, −0.12 eV, −0.12 eV, and −0.05 eV, respectively.[27] The trends from this prior work show very good agreement with our findings. As a result, NH_3 has the strongest interaction with Ti_2CO_2 with an E_{ad} of −0.37 eV, where N of NH_3 binds at the atop Ti site with a distance of 2.43 Å. The Ti atom that binds with N moves upwards slightly to the surface. Whereas the rest of the gas species have weak binding interactions with Ti_2CO_2.

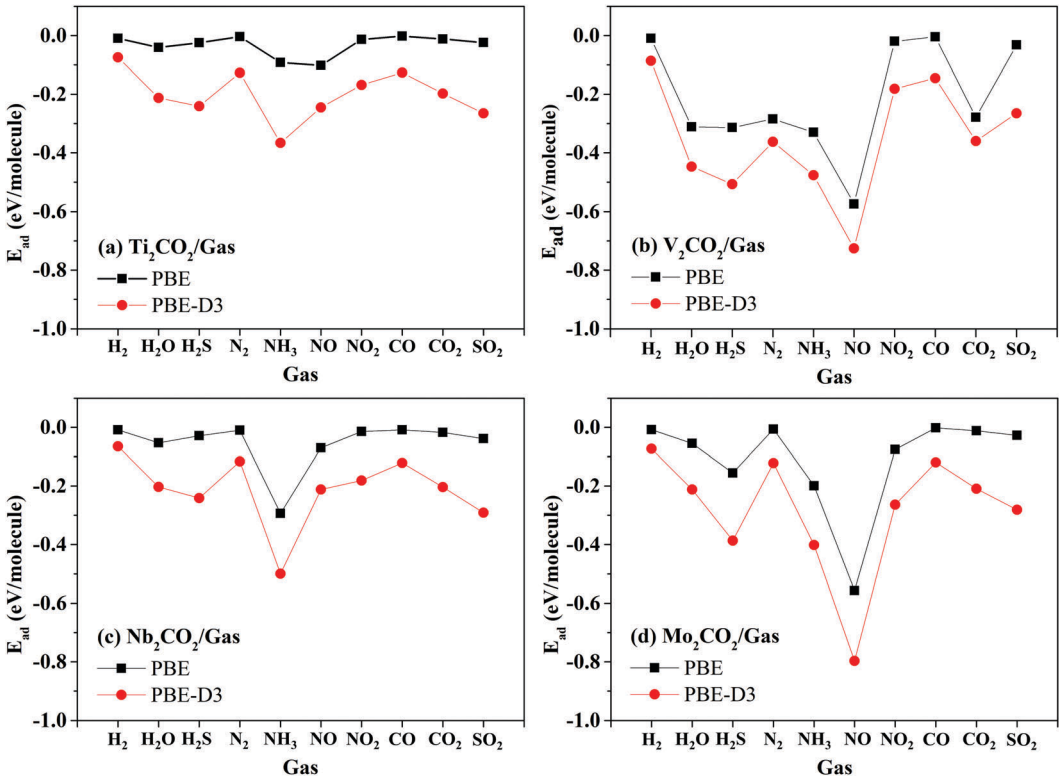

Fig. 4 Comparison of the E_{ad} values of gas adsorption on (a) Ti_2CO_2, (b) V_2CO_2, (c) Nb_2CO_2 and (d) Mo_2CO_2. Black squares and red circles represent the results calculated by the PAWPBE and (b) PAWPBE-D3 methods, respectively.

NO and SO_2 prefer the O sites and present an E_{ad} of about −0.25 eV. With the same adsorption configuration, an E_{ad} of SO_2/Ti_2CO_2 is slightly lower than an E_{ad} of −0.20 eV obtained from the DFT-D2 calculation results in the literature.[29] H_2S and H_2O bind with the O sites of Ti_2CO_2 by their hydrogen atoms with an E_{ad} of −0.21 eV and −0.24 eV, respectively. CO_2, NO_2, CO, N_2 and H_2 have an E_{ad} higher than −0.2 eV. Among the ten gas species, H_2 has the weakest interaction with an E_{ad} of −0.07 eV. This value is comparable with an E_{ad} of −0.05 eV from ref. 27. As a result, Ti_2CO_2 has good selectivity towards NH_3, which agrees well with prior work.[27]

The calculated E_{ad} values of the ten gas molecules on V_2CO_2 are compared in Fig. 4b. The calculated E_{ad} values and structures of the gas-adsorbed V_2CO_2 systems are given in Table S1 and Fig. S6 in the ESI.† According to the calculated E_{ad} values, the adsorption strengths are in the following order: NO/V_2CO_2 (E_{ad} = −0.73 eV) > H_2S/V_2CO_2 (E_{ad} = −0.51 eV) > NH_3/V_2CO_2 (E_{ad} = −0.48 eV) > H_2O/V_2CO_2 (E_{ad} = −0.45 eV) > N_2/V_2CO_2 (E_{ad} = −0.36 eV) ≈ CO_2/V_2CO_2 (E_{ad} = −0.36 eV) > SO_2/V_2CO_2 (E_{ad} = −0.27 eV) > NO_2/V_2CO_2 (E_{ad} = −0.18 eV) > CO/V_2CO_2 (E_{ad} = −0.14 eV) > H_2/V_2CO_2 (E_{ad} = −0.09 eV). The strongest adsorption strength can be observed in the NO/V_2CO_2 system with an E_{ad} of −0.73 eV. N of NO attached with the O site of the surface with a distance of 2.27 Å. The O–N–O angle is 109.2°. Similar to the Ti_2CO_2 case, H_2S and H_2O form an H–O interaction with the O sites on the surface with distances of about 2.3 to 2.4 Å. In the case of NO_2, CO and SO_2, they have weak interactions with the surface. Mostly, the binding strength of each gas on V_2CO_2 is enhanced compared to that of the Ti_2CO_2 surface. Likewise, H_2 shows the least binding strength with the surface compared to the other gas molecules. As a result, V_2CO_2 is selective towards NO.

Next, the gas adsorption on Nb_2CO_2 is considered. The results are compared in Fig. 4c. Fig. S7 (ESI†) presents the calculated E_{ad} values and relevant structures of the gas-adsorbed Nb_2CO_2 systems. The adsorption strength is in the following order: NH_3/Nb_2CO_2 (E_{ad} = −0.50 eV) > SO_2/Nb_2CO_2 (E_{ad} = −0.29 eV) > H_2S/Nb_2CO_2 (E_{ad} = −0.24 eV) > NO/Nb_2CO_2 (E_{ad} = −0.21 eV) > CO_2/Nb_2CO_2 (E_{ad} = −0.20 eV) ≈ H_2O/Nb_2CO_2 (E_{ad} = −0.20 eV) > NO_2/Nb_2CO_2 (E_{ad} = −0.18 eV) > CO/Nb_2CO_2 (E_{ad} = −0.12 eV) ≈ N_2/Nb_2CO_2 (E_{ad} = −0.12 eV) > H_2/Nb_2CO_2 (E_{ad} = −0.06 eV). Among the ten molecules, NH_3 has the strongest interaction with Nb_2CO_2 (E_{ad} of −0.50 eV) compared to the others. N of NH_3 binds with the Nb site with a distance of 2.41 Å. The configurations of H_2O and H_2S on the Nb_2CO_2 surface and their E_{ad} values are similar to those on the Ti_2CO_2 surface. The E_{ad} values of the other gases are in the range of −0.30 to −0.05 eV. Physisorption can be identified as the structures of the gas molecules are not distorted. Thus, Nb_2CO_2 provides good selectivity towards NH_3. It is worth noting that Nb_2CO_2 has stronger interactions with NH_3 than Ti_2CO_2.

For the last system, the plots of E_{ad} values of gas adsorption on Mo_2CO_2 are displayed in Fig. 4d. The detailed results of gas-adsorbed Mo_2CO_2 are summarized in Table S1 and Fig. S8 (ESI†). According to the calculated E_{ad} values, the tendency of binding strength between the gas and the surface is in the

following order: NO/Mo_2CO_2 (E_{ad} = −0.80 eV) > NH_3/Mo_2CO_2 (E_{ad} = −0.40 eV) ≈ H_2S/Mo_2CO_2 (E_{ad} = −0.39 eV) > SO_2/Mo_2CO_2 (E_{ad} = −0.28 eV) > NO_2/Mo_2CO_2 (E_{ad} = −0.26 eV) > H_2O/Mo_2CO_2 (E_{ad} = −0.21 eV) ≈ CO_2/Mo_2CO_2 (E_{ad} = −0.21 eV) > CO/Mo_2CO_2 (E_{ad} = −0.12 eV) ≈ N_2/Mo_2CO_2 (E_{ad} = −0.12 eV) > H_2/Mo_2CO_2 (E_{ad} = −0.07 eV). Mo_2CO_2 shows a similar aspect as V_2CO_2 that it binds with NO better than the other nine molecules. Additionally, the configuration of NH_3 on Mo_2CO_2 is different from other O-MXenes. Three H atoms of NH_3 interact with the O sites of the substrate. NO/Mo_2CO_2, NH_3/Mo_2CO_2 and H_2S/Mo_2CO_2 have E_{ad} values lower than −0.4 eV, while the rest have an E_{ad} greater than −0.3 eV. Mo_2CO_2 is selective towards NO. The interaction between NO and Mo_2CO_2 is slightly stronger than that in the Nb_2CO_2 system.

Although the PBE and PBE-D3 methods present similar bond lengths and configurations for the clean surfaces (*i.e.* bare M_2C and bare M_2CO_2), the dispersion contribution in the PBE-D3 calculation enhances the adsorption strength compared with the PBE calculation. In the adsorption complexes, E_{ad} can be decreased about 0.1 eV to 0.3 eV, when D3 correction is included. The variation of configurations is different depending on the systems. A comparison of the results from the PBE and PBE-D3 calculations of the four favourable systems is given in Table S2 in the ESI.† For the NH_3/Ti_2CO_2 and NH_3/Nb_2CO_2 cases, both the O′–H and metal–N interactions contribute to the NH_3 adsorption on these surfaces. In NO/V_2CO_2, the distance between NO and the substrate is decreased about 0.06 Å, when D3 correction is included. In NO/Mo_2CO_2, the adsorbed configurations calculated using the PBE and PBE-D3 methods are different, as more distortion of the Mo_2CO_2 surface can be observed in the PBE calculation. The O′–Mo^2 distance of the Mo_2CO_2 substrate is longer than that of other O′–Mo bonds (see Table S2 and Fig. S9 in the ESI†). The $r_{(M-O)}$ and $r_{(M-C)}$ values in Table S2 (ESI†) are changed from those of their clean surfaces (see Table 1) due to the interaction between the substrates and gas molecules. Furthermore, the adsorption energy difference (ΔE_{ad}) and the atomic distance difference (Δr) of the closest interacting points between a substrate and an adsorbate are given in Table S3 in the ESI.† Among the ten molecules, the dispersion shows more contribution on the adsorption energy of H_2O, H_2S, NH_3, CO_2 and SO_2 in most O-MXenes. The change in the adsorption strength *via* the inclusion of van der Waals forces also corresponds to the adsorption configuration (*i.e.* the number of bonds between an adsorbate and an adsorbent) of each gas–substrate complex. For example, the dispersion contribution from one Ti′–N and three O–H influences the adsorption between NH_3 and Ti_2CO_2 as illustrated in Fig. S9 (ESI†). By including D3, the atomic distances are changed slightly in all cases except for H_2S/Ti_2CO_2 and H_2S/V_2CO_2.

As shown in Fig. 4, Mo_2CO_2 and V_2CO_2 present good selectivity towards NO, while Nb_2CO_2 and Ti_2CO_2 show good selectivity towards NH_3. NO and NH_3 prefer binding with oxygen and metal sites, respectively. H_2, N_2, CO, CO_2, NO_2, and SO_2 are weakly bound on most O-MXenes. H_2 shows the weakest adsorption strength (E_{ad} > −0.1 eV) in all cases. In summary, the interactions between gases and O-MXenes in this work are dominated by the physisorption process. This physisorption characteristic can be identified from both the magnitudes of E_{ad} and also the structures of the adsorbed gases which are similar to their gas phase. The structures of the four O-MXenes are not distorted upon gas adsorption. This is a desired property of re-usable adsorbents. In addition, the strong binding energy of oxygen on the MXenes can explain the high stability of the O-MXenes that can prevent oxygen loses during usage. They tend to be stable at a high temperature. Owing to E_{ad}, SO_2 is weakly adsorbed on the O-MXenes. This aspect indicates that O-MXenes are very selective towards SO_2 which is a corrosive gas in gas streams. These aforementioned features are broadening the use of these O-functionalized MXenes in various applications. The electronic charge properties are discussed in the next section in order to understand more about the interaction between the gas and O-MXenes and also their pre-adsorbed structures.

3.4 Electronic charge properties

The electronic charge analyses of NH_3/Ti_2CO_2, NH_3/Nb_2CO_2, NO/V_2CO_2 and NO/Mo_2CO_2 are discussed in this section. First, charge transfer was obtained by performing Bader charge calculations. The positive and negative values of Bader charge change (Δe^-) denote the increment and the decrement of total valence electrons compared to their neutral states, respectively. On the other hand, a positive value of Δe^- indicates that an atom/molecule gains electrons and becomes a negative partial charge and *vice versa*. The calculated Δe^- and selected atomic distances are given in Table 2.

It is to be noted that the Bader charge changes given in Table 2 are the total charge change of a substrate and the total charge change of an adsorbate of each adsorption complex. As a result, electrons are donated from the gas species to the substrates in all four cases. For NH_3/Ti_2CO_2, electrons transfer from NH_3 to Ti_2CO_2 ~ $0.15e^-$. This result is comparable with $0.17e^-$ from ref. 27. Similarly, NH_3 transfers its electrons to Nb_2CO_2 about $0.14e^-$. In the latter cases, electrons are transferred from NO to V_2CO_2 and Mo_2CO_2 about $0.26e^-$ and $0.38e^-$, respectively.

Table 2 Bader charge analyses of gas adsorbed O-MXenes, selected atomic distances (r) in Å and angle (∠) in degree (°) calculated by PAWPBE-D3. Prime (′) represents an atom of O-MXene

	Bader charge		Atomic distance	
System	Atom	(Δe^-)	Atoms	r (Å)
NH_3/Ti_2CO_2	Ti_2CO_2	+0.15	Ti′–N	2.43
(E_{ad} = −0.37 eV)	NH_3	−0.15	N–H	1.02
NH_3/Nb_2CO_2	Nb_2CO_2	+0.14	Nb′–N	2.41
(E_{ad} = −0.50 eV)	NH_3	−0.14	N–H	1.02
NO/V_2CO_2	V_2CO_2	+0.26	O′–N	2.27
(E_{ad} = −0.73 eV)	NO	−0.26	N–O	1.15
			∠O′–N–O	109.21°
NO/Mo_2CO_2	Mo_2CO_2	+0.38	O′–N	2.11
(E_{ad} = −0.80 eV)	NO	−0.38	N–O	1.14
			∠O′–N–O	109.17°

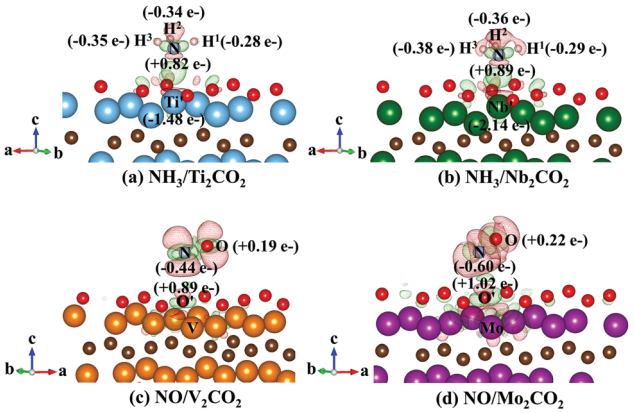

Fig. 5 Isosurface of charge difference and Bader charge values of (a) NH_3/Ti_2CO_2, (b) NH_3/Nb_2CO_2, (c) NO/V_2CO_2 and (d) NO/Mo_2CO_2. Green and red isosurfaces represent the increment and depletion of electrons, respectively. The isosurface values are ± 0.0035 e Å^{-3} and ± 0.002 e Å^{-3} in (a), (b) (c), and (d), respectively.

Moreover, the charge differences and Bader charge change of selected atoms of NH_3/Ti_2CO_2, NH_3/Nb_2CO_2, NO/V_2CO_2 and NO/Mo_2CO_2 are shown in Fig. 5a–d, accordingly. The accumulation and depletion of electrons are represented by the green and red regions, respectively. In Fig. 5a and b, the accumulation of electrons between N and the metal sites identifies the interaction between them. The Ti and Nb atoms become partially positive due to of the loss of their valence electrons upon adsorption. Although the total charge transfer between the NH_3 molecule and Nb_2CO_2 is slightly lower than that in NH_3/Ti_2CO_2 (see Table 2), the Δe^- of an individual N atom in NH_3/Ti_2CO_2 is lower than that of NH_3/Nb_2CO_2. Also, Nb reveals a more positive charge than Ti, which results in a stronger adsorption strength. In the latter two cases, the charge increment can also be observed between N of NO and O′ of the surfaces (see Fig. 5c and d). From Table 2 and Fig. 5, the shorter distances and more electron transfer between gas species and the substrates can be clearly observed in NO/V_2CO_2 and NO/Mo_2CO_2 compared to NH_3/Ti_2CO_2 and NH_3/Nb_2CO_2. The O atom of Mo_2CO_2 gains more electrons than that in NO/Mo_2CO_2 as presented in Fig. 5c and d. This evidence relates to the stronger binding interaction in NO/Mo_2CO_2 compared to other cases. In summary, the amount of charge transfer relates to the degree of adsorption strength and the distances between gas species and the substrates.

Furthermore, the projected density of states (PDOS) of valence electrons were ascertained out to understand the insight of the interaction and electronic charge nature of the systems. Fermi energy (E_F) is at zero. The PDOS plots of NH_3/Ti_2CO_2, NH_3/Nb_2CO_2, NO/V_2CO_2 and NO/Mo_2CO_2 are compared in Fig. 6. In each system, the PDOS plots of pristine MXene, pristine O-MXene and gas-adsorbed O-MXene are demonstrated in panel i to iii, respectively. Fig. 6a presents the PDOS plots of NH_3/Ti_2CO_2 and its clean Ti_2CO_2 and Ti_2C. The bonds between Ti, C and/or O atoms are indicated by the overlapping peaks of Ti_2C (panel i) and Ti_2CO_2 (panel ii and iii). For pristine Ti_2C, there is no gap existing at the Fermi level (E_F) as illustrated in panel i. This feature identifies the metallic nature of Ti_2C. However, the band gap can be observed upon the functionalization of Ti_2C with oxygen (see panel ii). Ti_2CO_2 has a band gap (E_g) of $\sim$0.32 eV, thus it becomes a semiconductor. The metallic and semiconducting characteristics of Ti_2C and Ti_2CO_2 observed in this work agree well with the results observed by other theoretical works.[10,14,27,53] For Ti_2CO_2, the E_g values of 0.24 eV[53] and 0.32 eV[15] were theoretically predicted by using the PBE functional. Generally, the DFT calculation underestimates the band gap (E_g) due to the self-interaction error inherent. The hybrid functional and GW approach have been used to attain more accurate E_g.[67,68] By using the HSE06 hybrid functional, the E_g values are predicted to be 0.88 eV[53] and 1.28 eV.[14] In the experiment, the O-terminated Ti_2C films (Ti_2CO_x) are semiconductors with $E_g \sim 80$ meV reported by Lai *et al.*[19] When NH_3 is adsorbed on the Ti_2CO_2 surface (see panel iii), the PDOS peaks of the substrates are almost the same as the pre-adsorbed one. There are extra peaks of conduction states presented at around 3.1–3.5 eV. Broadening of the PDOS peaks of NH_3 can be observed as it interacts with the Ti site. The overlapping PDOS peaks of NH_3 and Ti_2CO_2 at the energy level at around -2.5 eV corresponds well with those in ref. 27.

In the second system, the PDOS plots of NH_3/Nb_2CO_2 and the pristine surfaces are shown in Fig. 6b. Likewise, Nb_2C has the metallic characteristic without a band gap present at E_F as illustrated in panel i. Unlike Ti_2CO_2, Nb_2CO_2 retains the metallic feature (see panel ii). Hybridization of the PDOS peaks of Nb, C and O identifies bonding of those atoms of Nb_2CO_2. In addition, the PDOS peaks of Nb and C are broadened when Nb_2C is terminated by O atoms. In the NH_3 adsorption case, the presence of the PDOS peaks of NH_3 can be observed at the energy level below -3 eV as depicted in panel iii. Next, panel i to iii in Fig. 6c compare the PDOS plots of V_2C, V_2CO_2 and NO/V_2CO_2. Similar to the Nb_2CO_2 case, V_2CO_2 retains the metallic feature upon functionalization. This metallic behaviour of V_2CO_2 agrees with ref. 56. The bond between metal and C atoms are indicated by the hybridization of states. In panel iii, the peaks of NO present near E_F. The overlapping states also signify the interaction between the gas and the substrate. For the NO-adsorbed Mo_2CO_2 system, the relevant PDOS plots are compared in Fig. 6d. The hybridization of the PDOS peaks of the constituents can be observed. In panel iii, the existing PDOS peaks of NO near E_F can be observed as the same as those of NO/V_2CO_2. In summary, all pristine MXenes show metallic behaviors as shown in panel (i) in each case. All the O-functionalized surfaces also present the metallic nature except Ti_2CO_2. In the literature, MXenes that change from metal to semiconductor upon functionalization are Hf_2CO_2, Zr_2CO_2, Sc_2CO_2 and Sc_2CF_2.[14]

It is noteworthy that our calculated results (*i.e.* E_{ad} and electronic charge properties) of gas-adsorbed Ti_2CO_2 agree very well with the results of Yu *et al.*[27] In that study, the authors also applied the nonequilibrium Green's function (NEGF) method to predict the current–voltage (I–V) relations before and after the NH_3 adsorption on Ti_2CO_2. Their simulated results show

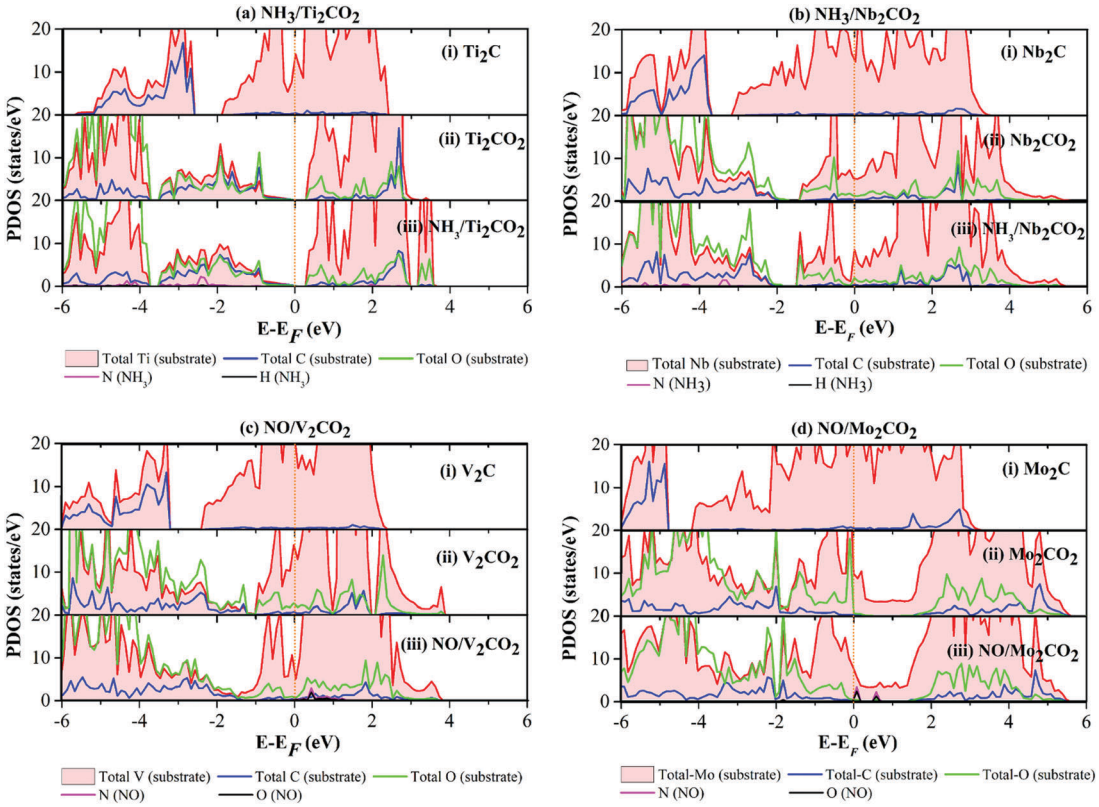

Fig. 6 PDOS of the (a) NH_3/Ti_2CO_2, (b) NH_3/Nb_2CO_2, (c) NO/V_2CO_2 and (d) NO/Mo_2CO_2 systems. In each system PDOS of the pristine M_2C (panel i), the pristine M_2CO_2 (panel ii) and the gas/M_2CO_2 (panel iii) are compared.

that Ti_2CO_2 has good sensitivity towards NH_3. This agreement assures that the prediction of high selectivity of Nb_2CO_2 towards NH_3 and V_2CO_2 or Mo_2CO_2 toward NO in our work provides a good guidance for applying these O-MXenes in specific purposes such as gas capture, gas separation, catalysis, *etc.*

Nb_2CO_2 and Ti_2CO_2 can be applied in NH_3 sensing, -capture, -storage applications. For example, they would be tested as ammonia adsorbents to purify H_2 used in a hydrogen storage system,[69] since they express a better NH_3 adsorption ability over H_2. Likewise, their selectivity suggest that they might be good choices for NO treatment technologies such as a selective catalytic reduction of NO by NH_3 (NH_3-SCR of NO) and NOx storage/reduction (NSR) methods.[70] Ti_2CO_2 and Nb_2CO_2 are recommended for further investigation in the NH_3-SCR of NO application, since this reaction requires NH_3 adsorption in an initial step. Besides, V_2CO_2 and Mo_2CO_2 might be tested for NO oxidation, since it tends to form NO_2 with O atoms on those O-MXenes. On the other hand, forming oxygen vacancies or controlling the oxygen coverage on O-functionalized MXenes might be used for catalytic applications. As presented in the previous investigation, Ti_2CO_2 with an oxygen vacancy (O_v) provided a good catalytic performance when converting CO_2 into HCOOH.[16] Additionally, these O-MXenes are tolerant to SO_2, which is a corrosive gas in gas streams. The terminating oxygen atoms also exhibit high stability on their surfaces. These properties are desirable for using these materials in practical applications.

4. Conclusions

Plane wave-based DFT calculations were used to investigate the adsorption of gas molecules on four MXenes and their O-functionalized surfaces. Not only the energetic and structural properties, but also the electronic charge properties were characterized and were used to explain their natures. On bare MXenes, most molecules are dissociated upon the adsorption process. The predominant chemisorption process with low adsorption energy indicates high reactivity of MXenes but low selectivity towards these gas molecules. Among the eleven gas molecules, only NH_3 is molecularly adsorbed on these four MXenes. For CO and N_2, they are not completely dissociated but their bonds are activated when they are adsorbed on MXenes. These characteristics reveal that bare MXenes might be possible catalysts for CO_2 conversion or nitrogen fixation to ammonia. In contrast to their bare surfaces, the O-functionalized MXenes show a weaker gas adsorption strength than pristine MXenes, but they are more selective towards particular gas species. Based on the calculated adsorption energies, Ti_2CO_2 and Nb_2CO_2 adsorb NH_3 stronger than others while Mo_2CO_2 and V_2CO_2 prefer NO. In addition, the PDOS and ELF properties can clearly describe the nature of MXenes and O-MXenes. The analyzed electronic charge properties demonstrated the charge transfer from the gas to the substrates. In summary, the amount of charge transfer related to the degree of adsorption strength and the distances between gas species and the substrates.

Our findings identify the feasibility of using O-MXenes in gas-separation, -capture, -sensing and catalytic applications. These O-MXenes reveal good stability and durability which are attractive when using them in actual operating systems. The results help to narrow down the choices of candidates for future experimental work. The outcome also provides more insights into these new 2D materials.

Conflicts of interest

There is no conflict to declare.

Acknowledgements

A. J. acknowledges the financial support from the National Nanotechnology Center (NANOTEC) through grant P1750381. R. A. acknowledges the partial support of NSF through grants DMR-1410983 and CMMI-1729335 (Collaborative Research: Accelerated Development of Damage Tolerant and Oxidation Resistant Alumina-Forming MAX Phases). Most of the calculations were carried out on the computer facilities of National e-Science Infrastructure Consortium, Thailand, and the STAMPEDE clusters of Texas Advanced Computing Center (TACC) at the University of Texas at Austin.

References

1 A. C. Dillon and M. J. Heben, *Appl. Phys. A: Mater. Sci. Process.*, 2001, **72**, 133–142.
2 K. Ramasubramanian, Y. Zhao and W. S. Winston Ho, *AIChE J.*, 2013, **59**, 1033–1045.
3 F. Rezaei, A. A. Rownaghi, S. Monjezi, R. P. Lively and C. W. Jones, *Energy Fuels*, 2015, **29**, 5467–5486.
4 K. Toda, R. Furue and S. Hayami, *Anal. Chim. Acta*, 2015, **878**, 43–53.
5 H. Li, J. Shang, Z. Ai and L. Zhang, *J. Am. Chem. Soc.*, 2015, **137**, 6393–6399.
6 C. Tan, X. Cao, X.-J. Wu, Q. He, J. Yang, X. Zhang, J. Chen, W. Zhao, S. Han, G.-H. Nam, M. Sindoro and H. Zhang, *Chem. Rev.*, 2017, **117**, 6225–6331.
7 Q. Tang and Z. Zhou, *Prog. Mater. Sci.*, 2013, **58**, 1244–1315.
8 A. Molle, J. Goldberger, M. Houssa, Y. Xu, S.-C. Zhang and D. Akinwande, *Nat. Mater.*, 2017, **16**, 163–169.
9 L. Shi and T. Zhao, *J. Mater. Chem. A*, 2017, **5**, 3735–3758.
10 M. Khazaei, A. Ranjbar, M. Arai, T. Sasaki and S. Yunoki, *J. Mater. Chem. C*, 2017, **5**, 2488–2503.
11 V. M. Hong, Ng, H. Huang, K. Zhou, P. S. Lee, W. Que, J. Z. Xu and L. B. Kong, *J. Mater. Chem. A*, 2017, **5**, 3039–3068.
12 B. Anasori, M. R. Lukatskaya and Y. Gogotsi, *Nat. Rev. Mater.*, 2017, **2**, 16098.
13 X. Ji, K. Xu, C. Chen, B. Zhang, Y. Ruan, J. Liu, L. Miao and J. Jiang, *Phys. Chem. Chem. Phys.*, 2016, **18**, 4460–4467.
14 Z. Guo, J. Zhou, L. Zhu and Z. Sun, *J. Mater. Chem. A*, 2016, **4**, 11446–11452.
15 A. N. Gandi, H. N. Alshareef and U. Schwingenschlögl, *Chem. Mater.*, 2016, **28**, 1647–1652.
16 X. Zhang, Z. Zhang, J. Li, X. Zhao, D. Wu and Z. Zhou, *J. Mater. Chem. A*, 2017, **5**, 12899–12903.
17 M. Naguib, M. Kurtoglu, V. Presser, J. Lu, J. Niu, M. Heon, L. Hultman, Y. Gogotsi and M. W. Barsoum, *Adv. Mater.*, 2011, **23**, 4248–4253.
18 J. Li, Y. Du, C. Huo, S. Wang and C. Cui, *Ceram. Int.*, 2015, **41**, 2631–2635.
19 S. Lai, J. Jeon, S. K. Jang, J. Xu, Y. J. Choi, J.-H. Park, E. Hwang and S. Lee, *Nanoscale*, 2015, **7**, 19390–19396.
20 M. Naguib, O. Mashtalir, J. Carle, V. Presser, J. Lu, L. Hultman, Y. Gogotsi and M. W. Barsoum, *ACS Nano*, 2012, **6**, 1322–1331.
21 M. Naguib, J. Halim, J. Lu, K. M. Cook, L. Hultman, Y. Gogotsi and M. W. Barsoum, *J. Am. Chem. Soc.*, 2013, **135**, 15966–15969.
22 R. Meshkian, L.-Å. Näslund, J. Halim, J. Lu, M. W. Barsoum and J. Rosen, *Scr. Mater.*, 2015, **108**, 147–150.
23 J. Zhou, X. Zha, F. Y. Chen, Q. Ye, P. Eklund, S. Du and Q. Huang, *Angew. Chem., Int. Ed.*, 2016, **55**, 5008–5013.
24 J. Yang, M. Naguib, M. Ghidiu, L.-M. Pan, J. Gu, J. Nanda, J. Halim, Y. Gogotsi and M. W. Barsoum, *J. Am. Ceram. Soc.*, 2016, **99**, 660–666.
25 P. Urbankowski, B. Anasori, T. Makaryan, D. Er, S. Kota, P. L. Walsh, M. Zhao, V. B. Shenoy, M. W. Barsoum and Y. Gogotsi, *Nanoscale*, 2016, **8**, 11385–11391.
26 M. Khazaei, M. Arai, T. Sasaki, C.-Y. Chung, N. S. Venkataramanan, M. Estili, Y. Sakka and Y. Kawazoe, *Adv. Funct. Mater.*, 2013, **23**, 2185–2192.
27 X.-F. Yu, Y.-C. Li, J.-B. Cheng, Z.-B. Liu, Q.-Z. Li, W.-X. Li, X. Yang and B. Xiao, *ACS Appl. Mater. Interfaces*, 2015, **7**, 13707–13713.
28 B. Xiao, Y.-C. Li, X.-F. Yu and J.-B. Cheng, *Sens. Actuators, B*, 2016, **235**, 103–109.
29 S. Ma, D. Yuan, Z. Jiao, T. Wang and X. Dai, *J. Phys. Chem. C*, 2017, **121**, 24077–24084.
30 E. Lee, A. VahidMohammadi, B. C. Prorok, Y. S. Yoon, M. Beidaghi and D.-J. Kim, *ACS Appl. Mater. Interfaces*, 2017, **9**, 37184–37190.
31 J. Zhu, E. Ha, G. Zhao, Y. Zhou, D. Huang, G. Yue, L. Hu, N. Sun, Y. Wang, L. Y. S. Lee, C. Xu, K.-Y. Wong, D. Astruc and P. Zhao, *Coord. Chem. Rev.*, 2017, **352**, 306–327.
32 L. Wang, L. Yuan, K. Chen, Y. Zhang, Q. Deng, S. Du, Q. Huang, L. Zheng, J. Zhang, Z. Chai, M. W. Barsoum, X. Wang and W. Shi, *ACS Appl. Mater. Interfaces*, 2016, **8**, 16396–16403.
33 Y.-J. Zhang, Z.-J. Zhou, J.-H. Lan, C.-C. Ge, Z.-F. Chai, P. Zhang and W.-Q. Shi, *Appl. Surf. Sci.*, 2017, **426**, 572–578.
34 A. Shahzad, K. Rasool, W. Miran, M. Nawaz, J. Jang, K. A. Mahmoud and D. S. Lee, *ACS Sustainable Chem. Eng.*, 2017, **5**, 11481–11488.
35 M. R. Lukatskaya, O. Mashtalir, C. E. Ren, Y. Dall'Agnese, P. Rozier, P. L. Taberna, M. Naguib, P. Simon, M. W. Barsoum and Y. Gogotsi, *Science*, 2013, **341**, 1502.
36 Y. Dall'Agnese, P.-L. Taberna, Y. Gogotsi and P. Simon, *J. Phys. Chem. Lett.*, 2015, **6**, 2305–2309.

37 Y. Zhao and J. Zhao, *Appl. Surf. Sci.*, 2017, **412**, 591–598.
38 D. Zhang, M. Ashton, A. Ostadhossein, A. C. T. van Duin, R. G. Hennig and S. B. Sinnott, *ACS Appl. Mater. Interfaces*, 2017, **9**, 34467–34479.
39 B. D. Dunnington and J. R. Schmidt, *J. Catal.*, 2015, **324**, 50–58.
40 G. Kresse and J. Hafner, *Phys. Rev. B: Condens. Matter Mater. Phys.*, 1993, **47**, 558–561.
41 G. Kresse and J. Furthmüller, *Phys. Rev. B: Condens. Matter Mater. Phys.*, 1996, **54**, 11169–11186.
42 J. Paier, R. Hirschl, M. Marsman and G. Kresse, *J. Chem. Phys.*, 2005, **122**, 234102.
43 G. Kresse and D. Joubert, *Phys. Rev. B: Condens. Matter Mater. Phys.*, 1999, **59**, 1758–1775.
44 S. Grimme, J. Antony, S. Ehrlich and H. Krieg, *J. Chem. Phys.*, 2010, **132**, 154104.
45 E. Yang, H. Ji, J. Kim, H. Kim and Y. Jung, *Phys. Chem. Chem. Phys.*, 2015, **17**, 5000–5005.
46 J. Guo, Q. Peng, H. Fu, G. Zou and Q. Zhang, *J. Phys. Chem. C*, 2015, **119**, 20923–20930.
47 L. M. Azofra, N. Li, D. R. MacFarlane and C. Sun, *Energy Environ. Sci.*, 2016, **9**, 2545–2549.
48 J. Gebhardt, F. Vines, P. Bleiziffer, W. Hieringer and A. Gorling, *Phys. Chem. Chem. Phys.*, 2014, **16**, 5382–5392.
49 A. D. Becke and K. E. Edgecombe, *J. Chem. Phys.*, 1990, **92**, 5397–5403.
50 W. Tang, E. Sanville and G. Henkelman, *J. Phys.: Condens. Matter*, 2009, **21**, 084204.
51 M. Yu and D. R. Trinkle, *J. Chem. Phys.*, 2011, **134**, 064111.
52 H. Lashgari, M. R. Abolhassani, A. Boochani, S. M. Elahi and J. Khodadadi, *Solid State Commun.*, 2014, **195**, 61–69.
53 Y. Xie and P. R. C. Kent, *Phys. Rev. B: Condens. Matter Mater. Phys.*, 2013, **87**, 235441.
54 J. Hu, B. Xu, C. Ouyang, Y. Zhang and S. A. Yang, *RSC Adv.*, 2016, **6**, 27467–27474.
55 Q. Sun, Y. Dai, Y. Ma, T. Jing, W. Wei and B. Huang, *J. Phys. Chem. Lett.*, 2016, **7**, 937–943.
56 M. Khazaei, M. Arai, T. Sasaki, M. Estili and Y. Sakka, *Phys. Chem. Chem. Phys.*, 2014, **16**, 7841–7849.
57 S. Shaik, D. Danovich, B. Silvi, D. L. Lauvergnat and P. C. Hiberty, *Chem. – Eur. J.*, 2005, **11**, 6358–6371.
58 E. Matito, B. Silvi, M. Duran and M. Solà, *J. Chem. Phys.*, 2006, **125**, 024301.
59 B. Silvi, I. Fourré and M. E. Alikhani, *Monatsh. Chem.*, 2005, **136**, 855–879.
60 E. Matito and M. Solà, *Coord. Chem. Rev.*, 2009, **253**, 647–665.
61 G. J. Kubas, R. R. Ryan, B. I. Swanson, P. J. Vergamini and H. J. Wasserman, *J. Am. Chem. Soc.*, 1984, **106**, 451–452.
62 H. Valencia, A. Gil and G. Frapper, *J. Phys. Chem. C*, 2015, **119**, 5506–5522.
63 Q. Hu, D. Sun, Q. Wu, H. Wang, L. Wang, B. Liu, A. Zhou and J. He, *J. Phys. Chem. A*, 2013, **117**, 14253–14260.
64 L.-Y. Gan, D. Huang and U. Schwingenschlogl, *J. Mater. Chem. A*, 2013, **1**, 13672–13678.
65 K. D. Fredrickson, B. Anasori, Z. W. Seh, Y. Gogotsi and A. Vojvodic, *J. Phys. Chem. C*, 2016, **120**, 28432–28440.
66 N. Li, X. Chen, W.-J. Ong, D. R. MacFarlane, X. Zhao, A. K. Cheetham and C. Sun, *ACS Nano*, 2017, **11**, 10825–10833.
67 J. Hafner, *J. Comput. Chem.*, 2008, **29**, 2044–2078.
68 T. Yamamoto and T. Ohno, *Phys. Chem. Chem. Phys.*, 2012, **14**, 589–598.
69 B. A. van Hassel, J. R. Karra, J. Santana, S. Saita, A. Murray, D. Goberman, R. Chahine and D. Cossement, *Sep. Purif. Technol.*, 2015, **142**, 215–226.
70 S. Roy, M. S. Hegde and G. Madras, *Appl. Energy*, 2009, **86**, 2283–2297.

